Available online at www.sciencedirect.com
SCIENCE DIRECT®
International Journal of Mass Spectrometry 239 (2004) 1–6
International Journal of Mass Spectrometry
www.elsevier.com/locate/ijms

Distortion of ion trajectories in a time-of-flight mass spectrometer: simulations and experiments with a position sensitive detector

R. Antoine, L. Arnaud, M. Abd El Rahim, D. Rayane, M. Broyer, Ph. Dugourd*

Laboratoire de Spectrométrie Ionique et Moléculaire, UMR 5579, Université Lyon I et CNRS, 43 Bd du 11 Novembre 1918, 69622 Villeurbanne Cedex, France

Received 24 June 2004; accepted 27 August 2004
Available online 30 September 2004

Abstract

We used a position sensitive detector (PSD) to show the image of an ion packet at the end of a time-of-flight mass-spectrometer. The spread of the ion packet due to wires in the accelerator electrodes is directly observed on the image. A huge effect on the size and shape of the ion packet is observed. Experimental results are compared to SIMION simulations performed using a procedure developed to compute the trajectories of ions close to wires.

Keywords: Mass spectrometry; Time-of-flight; Ion imaging

1. Introduction

Grids and wires in accelerator electrodes and mirrors in time-of-flight mass-spectrometer (TOF-MS) instruments induce small deflections of ions. In addition to reduction in transmission, these deflections induce a spatial spread of the ion packet and lower the mass resolving power [1]. This spatial spread also makes it difficult to use grids in a system built to observe the position, shape or energy spread of an ion packet. To avoid this ion spread, high resolving TOF-MS are built with gridless accelerators and reflectors. Gridless accelerators are well adapted to MALDI-TOF (MALDI: matrix assisted laser desorption ionization) apparatus where the ions are generated on the acceleration electrode at a well defined electric potential, but they are difficult to couple to a molecular beam set-up where the ions are generated in a relatively large volume and with an initial kinetic energy spread. In molecular physics, many designs include grids or wires and the resulting ion spread must be taken into account for high resolving mass spectrometers, ion imaging or simply to get a maximum of ions at a detector. In 1989, Bergmann et al. [2] proposed a calculation of the trajectory of an ion in the vicinity of a wire and estimated the effects of grids on the mass resolution. The effect on the time-width of a peak in the mass spectrum and on the resolution was experimentally demonstrated [3,4] and is also observed [5,6] in SIMION simulations that take into account real grids or wires [7,8]. Recently, we have coupled a position sensitive detector (PSD) to a TOF-MS to measure the position of a beam in molecular beam deflection experiments. In the present work, we use this detector to observe an ion packet at the exit of the TOF-MS and to characterize the trajectories of the ions in the TOF. For the first time, the spread of the ion packet induced by wires is directly observed. Results are compared to SIMION simulations.

2. Experiment

The apparatus is a laser vaporization source coupled to an electric deflector and a TOF-MS. It is described in detail in references [9,10]. A schematic of the TOF-MS is shown in Fig. 1. It is an orthogonal acceleration linear time-of-flight

* Corresponding author. Tel.: +33 4 72 43 11 32; fax: +33 4 72 43 15 07.
E-mail address: dugourd@lasim.univ-lyon1.fr (Ph. Dugourd).

1387-3806/$ – see front matter © 2004 Elsevier B.V. All rights reserved.
doi:10.1016/j.ijms.2004.08.007

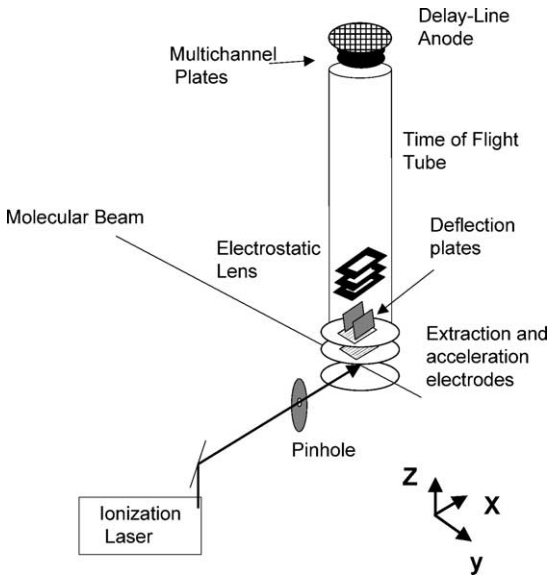

Fig. 1. Schematic of the TOF-MS-PSD instrument. The distance between the ionization laser axis and the detector is 1.375 m.

system. The MS is perpendicular to the axis of the neutral molecular beam and to the pulsed ionization laser. It consists of an extraction region, an acceleration region, two deflection plates, an electrostatic lens and a free flight region. Parallel wires are used to define the boundaries of the extraction and acceleration regions. We used 50 μm tungsten wires parallel to the *X*-axis. The spacing between two wires is 500 μm. They are glued onto a stainless steel plate with an aperture of 30 mm × 30 mm. Schematics of the extraction and acceleration electrodes and of the electrostatic lens are shown in Fig. 2. The detector is located 1.375 m downstream of the ionization laser axis. It is a pair of microchannel plates coupled to two orthogonal delay lines. The detector, its electronic and the data processing are discussed in [9].

Table 1
Electric fields (F_{Ext} and F_{Acc}) in the acceleration and extraction regions of the time-of-flight for the two sets of experimental acceleration and extraction voltages (U_{Ext} and U_{Acc})

	U_{Ext} (V)	U_{Acc} (V)	U_{Beam} (V)	F_{Ext} (10^3 V m^{-1})	F_{Acc} (10^3 V m^{-1})	U_D (V)
1	370	3500	3685	20.6	233.3	±70
2	2764	2303	3685	153.6	153.6	±40

The value of the voltages U_D applied on the two deflection electrodes and the voltage at the position of the molecular beam (U_{Beam}) are also given.

A glycine–tryptophan (Gly–Trp, M = 261) or alanine–tryptophan (Ala–Trp, M = 275) molecular beam was produced by vaporizing a rod made of 66% of cellulose and 33% of Gly–Trp or Ala–Trp (purchased from Bachem). The neutral beam is collimated by two 0.35 mm slits before entering the extraction region of the TOF-MS. The distances between the two slits, the second slit and the MS, are 0.6 and 1 m. The diameter of the ionization laser (λ = 266 nm, $\phi \sim 10$ mJ cm^{-2}) is 3 mm. Experiments were performed at two sets of extraction and acceleration voltages (the voltages and electric fields are summarized in Table 1). Mass spectra recorded for the Gly–Trp molecular beam are shown in Fig. 3. The first set of voltages corresponds to the Wiley–McLaren

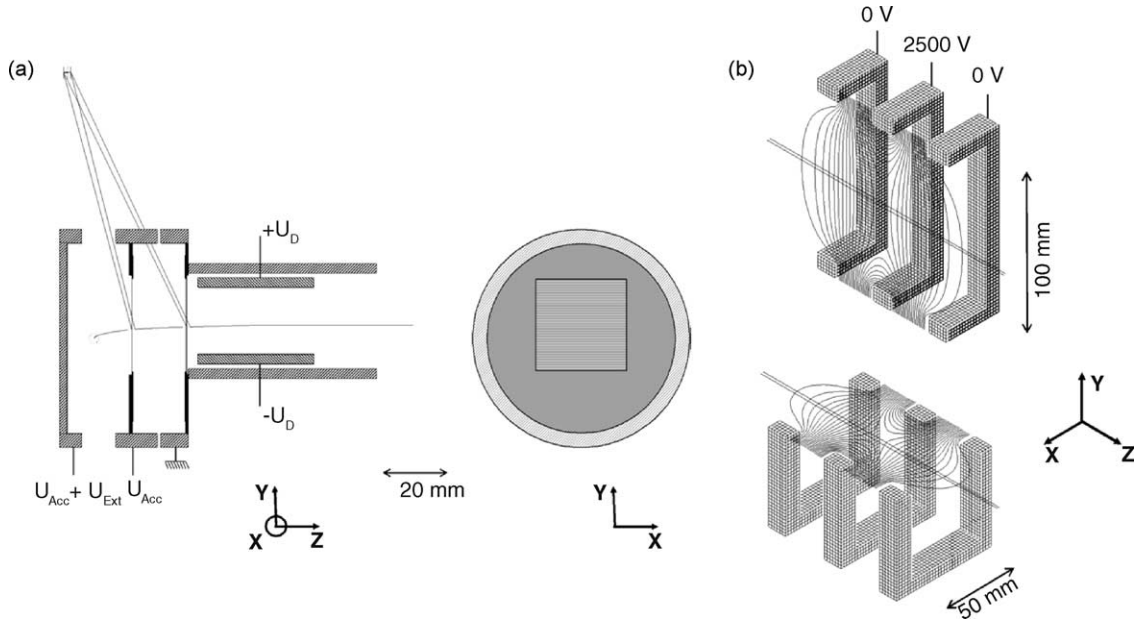

Fig. 2. (a) Left: schematic of the extraction and acceleration regions and of the deflection plates of the TOF–MS. The lengths of the extraction and acceleration regions are 18 and 15 mm. In SIMION simulations, the trajectory of an ion close to a wire is calculated using a specific potential array instance (see text). An example of ion trajectory in these regions is plotted (M = 261 amu, $v = 1485$ m s^{-1}, U_{Ext} = 370 V, U_{Acc} = 3500 V, U_D = ±70 V). Right: schematic of the acceleration electrode. (b) Schematic of the electrostatic lens. Equipotential lines in the *XZ* plane and the *YZ* plane are shown (the lines are separated by 100 V). Two examples of ion trajectories are also plotted.

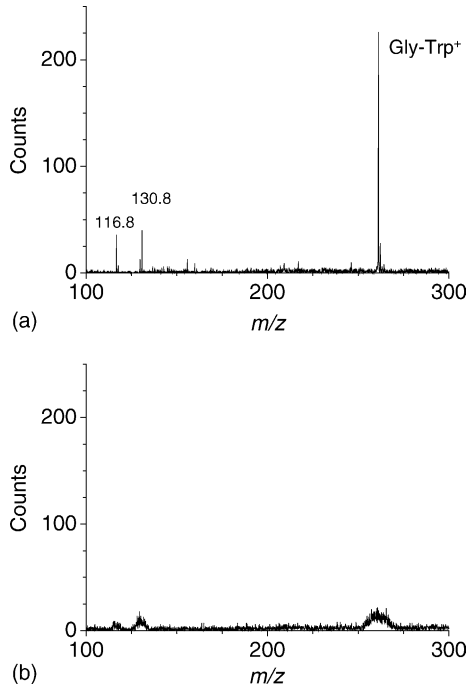

Fig. 3. TOF mass spectra recorded for Gly–Trp (M = 261). (a) U_{Ext} = 370 V, U_{Acc} = 3500 V. (b) U_{Ext} = 2764 V, U_{Acc} = 2303 V. The peaks on the left correspond to fragments.

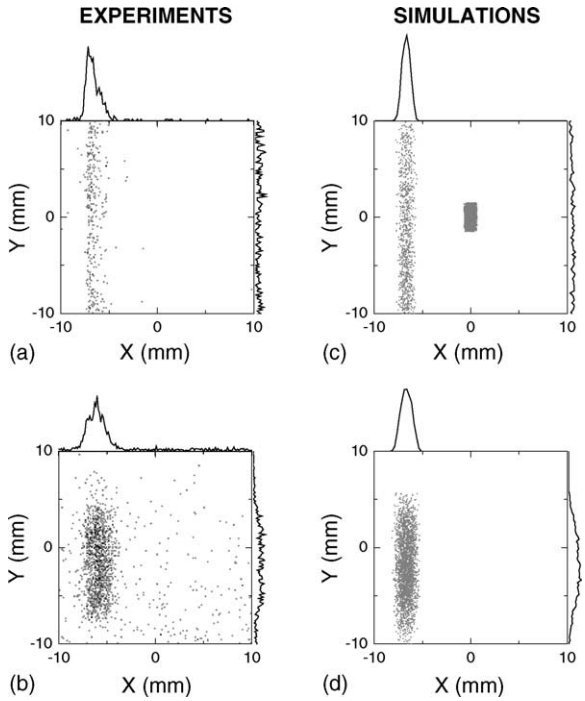

Fig. 4. Two-dimensional X–Y images of the Gly–Trp ions on the detector obtained with U_{Lens} = 0 V. The projections on the X-axis and Y-axis are also plotted. (a) Experimental results at the first set of voltages (Wiley–McLaren conditions, 513 ions were recorded). (b) Experimental results at the second set of voltages (1989 ions were recorded). (c and d) Results of SIMION simulations performed at the two set of voltages using experimental initial conditions. In (c), the initial ion packet used for the simulation is shown in the center of the image.

condition of time focusing [11]. The most intense peak in the mass spectrum (Fig. 3a) corresponds to Gly–Trp^+ ions. The peaks at 117 and 131 correspond to fragmentation products. These fragments may be assigned to indole derivatives: C_8H_7N (the indole molecule) and C_9H_9N (indole + CH_2).

The ion deflection depends mainly on the spacing between the wires and on the difference of the electric fields on the two sides of the wire layer [2]. To study the influence of the electric fields on the ion spread, a second set of voltages was chosen that produced equally large electric fields in the extraction and in the acceleration regions (F_{Ext} = F_{Acc}). In both cases, the ions have the same kinetic energies at the exit of the acceleration region for both sets of voltages (U_{Beam} in Table 1). For the second set of voltages (Fig. 3b), the mass resolution is low and broad peaks are observed in the time-of-flight mass spectrum.

Fig. 4a and b show X–Y images of the Gly–Trp ion packet obtained at the detector for the two sets of voltages. The width of the ion packet in X direction is similar in the two plots. This width reflects the initial width of the molecular beam. The ion packet is much wider in Y direction. In particular, with the Wiley–McLaren conditions, i.e. the first set of voltages in Table 1, no peak is observed on the Y-axis. The ions are regularly distributed along this axis. At the second set of voltages, a broad peak is observed in Y direction. The width of the peak is ∼12 mm. The spread on the Y-axis results from the formation of small electrostatic lenses between neighboring wires. These lenses disappear when the electric fields on the two sides of the wires are equal as is the case for the second set of voltages and, as expected, the experimentally observed spread is smaller.

Fig. 5a and b show images recorded for similar experimental conditions with the magnifying lens switched on (U_{Lens} = 2500 V). The lens magnifies (and shifts) the images in X direction with only a small effect in Y direction. This lens is important for imaging applications. It was designed to increase the width of the ion packet in X direction to increase the resolving power in molecular beam deflection experiments.

3. Simulations

The trajectories of the ions were simulated using SIMION 3D version 7.0 [8]. For the full system simulation, five separate arrays were used in order to keep a good scale factor (between 0.1 and 0.5 mm per grid unit) even for simulations of widely asymmetric regions. The exact shapes and thicknesses of the different electrodes were modeled in the simulation. Three potential arrays were used for the extraction, acceleration and deflection regions separated by grids which ensure convenient boundaries conditions. The overall enclosure of the TOFMS has been taken into account

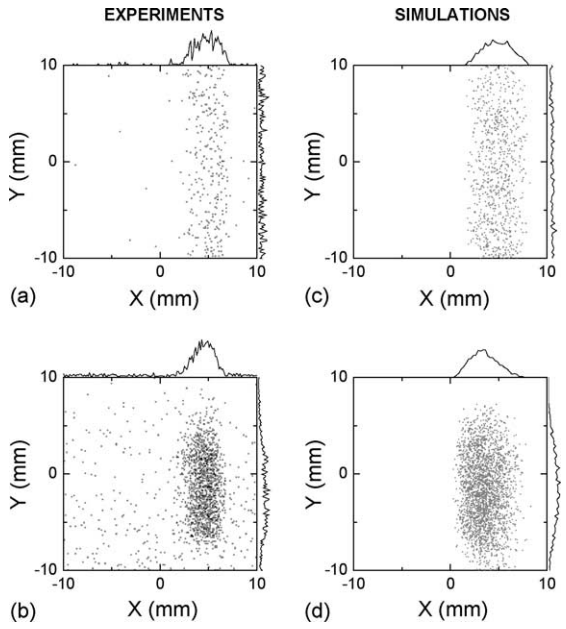

Fig. 5. 2D *X*–*Y* images of the Gly–Trp ions on the detector obtained with U_{Lens} = 2500 V. The projections on the *X*-axis and *Y*-axis are also plotted. (a) Experimental results at the first set of voltages (Wiley–McLaren conditions, 495 ions were recorded). (b) Experimental results at the second set of voltages (2379 ions were recorded). (c and d) Results of SIMION simulations performed at the two set of voltages using experimental initial conditions.

for realistic simulations of fringing fields of the electrostatic lens.

Wire scattering effects have been modeled with the approach described by Colby et al. for the simulation of grid lensing using instance hopping [7]. Based on the user program proposed by Colby, we developed a new program in which the real trajectory is taken into account when the ions fly near the wires and not only there is change in the direction but also its kinetic energy. This part of the trajectory is calculated in the non-ideal wires potential array (see Fig. 2). This potential array with a scale factor of 0.008 mm per grid unit enables us to properly describe the very small and closely spaced wires used in the experimental set-up.

The simulations were performed for an initial ion packet corresponding to the intersection of a rectangular (1.4 mm × 5 mm) molecular beam and a 3 mm diameter laser spot. The intensity profile of the beam in *X* direction is defined by the width and spacing of the slits. The initial packet used in the simulations is shown in Fig. 4c). The existing experimental conditions were used to define the initial velocity of the ions (v = 1485 ms^{-1} ± 2.5% with an angular spread of 0.5°). Three thousand initial ions were used in each simulation. The off-axis of the experimental image and the position shift induced by the lens were reproduced in the simulations by including very small rotations of the acceleration and extraction electrodes (0.28° around the *Y*-axis and 0.5° around the *X*-axis) and of the lens (−0.12° around the *Y*-axis) relative to each other.

4. Results and discussion

Results of the simulations are shown in Figs. 4c and d, 5c and d. All the experimental images with and without magnifying lens are qualitatively well reproduced. First, we discuss the wire effect in *Y* direction then the size of the image in *X* direction. The initial width of the ion packet in *Y* direction is given by the laser diameter (3 mm). In Fig. 4d, the width of the calculated image is ∼15 mm, which is in relatively good agreement with the experimental width (∼12 mm). At the Wiley–McLaren conditions, the size of the simulated image is ∼60 mm. This corresponds to an angular spread <15°. This width is larger than the aperture of the detector, which is in agreement with experimental results. The dramatic increase in *Y* spread with different fields on the two sides of the acceleration electrode is well reproduced by the simulation. This confirms the validity of the approach that we are using to simulate the wires effect. We want to emphasize that the spread induced by wires (or grids) is dramatic and that a small fraction of the initial ions hits the detector. No spread is expected in *X* direction. The initial width of the molecular beam is ∼1.4 mm. Without a lens (Fig. 4), the X size of the experimental image varies from ∼3 mm (set 1) to ∼4 mm (set 2) which is in relatively good agreement with the simulations (from ∼2 to 2.5 mm). The difference between the initial ion packet in the extraction region of the TOF-MS and the

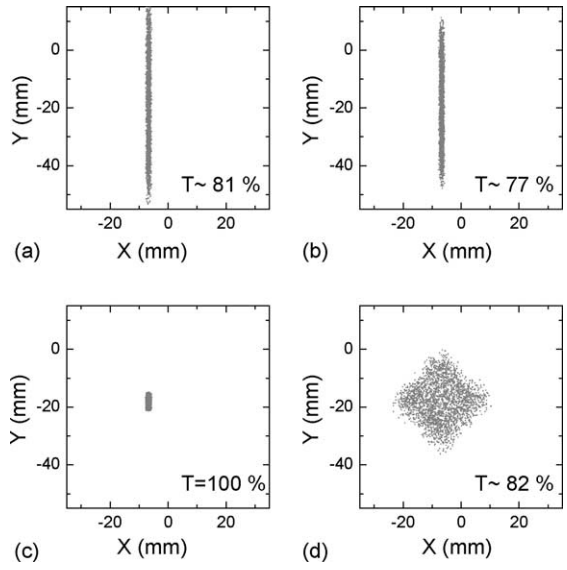

Fig. 6. Comparison of the influence of wire and grid effects on the size of the ion packet. *X*–*Y* images have been simulated for different extraction and acceleration electrodes (Gly–Trp ions, U_{Ext} = 370 V, U_{Acc} = 3500 V, U_D = ±70 V, U_{Lens} = 0 V). (a) Electrodes with wires (diameter: 50 μm, spacing between two wires: 500 μm) as used in the present work. (b) Electrodes with wires (diameter: 50 μm, spacing between two wires: 400 μm). (c) Electrodes with ideal grids (an ideal grid in SIMION simulations allows one to fix a potential without any ions spread and a transmission of 100%). (d) Typical grid with quadratic openings (round wires of 16 μm diameter and a spacing of 368 μm). The transmission through the extraction and acceleration plates is stated for each system.

image on the detector is due to a lens effect intrinsic to the acceleration region of the TOF. The uncertainty in the size of the initial ion packet, the spatial resolution of the detector, and a possible small divergence of the ion beam induced by space charge could explain the difference between the experiments and the simulations. The simulations (Fig. 5c and d) confirm that the magnifying lens has almost no effect in *Y* direction and increases the size of the image in *X* direction.

Fig. 6 compares the size of the ion packets at the end of the TOF-MS obtained in SIMION simulations for different spacing (400 and 500 μm) of the wires on the acceleration and extraction electrodes. A decrease in the spacing between the wires reduces the ion spread on the *Y*-axis. It also decreases the transmission of the plates. By reducing both the diameter and the spacing of the wires, it is possible to decrease the *Y* spread without change in transmission. For example, for 16 μm diameter wires and a spacing of 160 μm, one would obtain an image of 26 mm on the *Y*-axis and a transmission of 0.81. The use of grids instead of wires (Fig. 6d) would cause spreads on both axes. This figure clearly demonstrates that the initial size or shape of the ion packet is totally mixed up by the grids. It also confirms that it is possible to image the initial position or shape of the molecular beam in one direction by replacing the grids by wires.

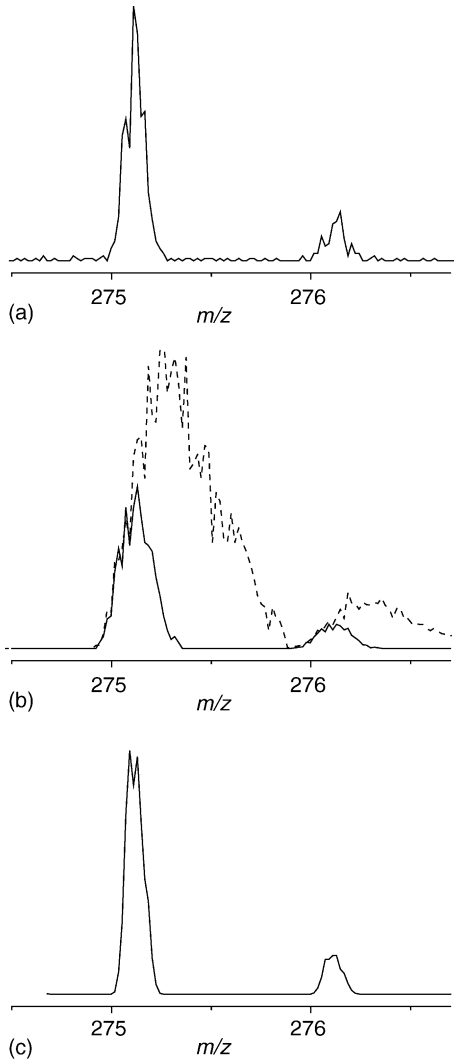

Fig. 7. TOF mass spectra of Ala–Trp$^+$ ions (U_{Ext} = 370 V, U_{Acc} = 3500 V, U_D = ±80 V, U_{Lens} = 2500 V). (a) Experimental. (b) Simulation—full line: only the ions that hit the detector are included in the simulation (504 ions for 3000 initial ions), dashed line: all the ions that are passing through wires are included (2435 ions for 3000 initial ions). (c) Simulation with ideal grids instead of real wires (an ideal grid in SIMION simulations allows one to fix a potential without any ions spread and a transmission of 100%, 3000 ions are used for the simulation).

Finally, Fig. 7 displays experimental and calculated mass spectra for Ala–Trp$^+$. The spectra are magnified to illustrate the mass resolution. Fig. 7c shows a calculated spectrum obtained with ideal grids to divide the extraction and acceleration regions in SIMION simulations instead of wires (definition of the voltages without ion spreads). The dashed line in Fig. 7b corresponds to the same spectrum obtained with wires in the simulation (the arrival time of all ions are taken into account to construct the spectrum). The comparison of the two spectra (dashed lines in Fig. 7b and 7c) shows that the spread of the ions by the wires drastically lowers the mass resolution; this is in agreement with previous publications. The size of the detector is smaller than the ion packet at the end of the detector. The full line corresponds to the spectrum obtained by taking into account in the calculation only the ions that impinge on the detector. The ions with the shorter trajectories are observed. A good resolution, in agreement with the experiment, is recovered. It is important to notice that this relatively good resolving power is obtained because only a small fraction of the ions is detected. The ion spread induced by wires or grids is clearly a limiting factor of the resolution for a TOF-MS without a reflector.

5. Conclusions

We have used a position sensitive detector to observe the image of an ion packet at the end of a linear TOF-MS. The spread of the ion packet due to wires in the accelerator is directly observed on the image. This spread is in agreement with SIMION simulations performed using a procedure developed to compute the trajectory of the ions near wires and grids. The use of wires on the extraction and acceleration plates allows us to image the position and shape of the beam in *X* direction with a good mass resolution.

Acknowledgements

The authors thank Anne Viard for help in taking the experimental data, I. Compagnon for the development of the new detection and M. Barbaire, Ch. Clavier and J. Maurelli for technical support.

References

[1] M. Guilhaus, D. Selby, V. Mlynski, Mass Spectrom. Rev. 19 (2000) 65.
[2] T. Bergmann, T.P. Martin, H. Schaber, Rev. Sci. Instrum. 60 (1989) 347.
[3] M. Guilhaus, V. Mlynski, D.S. Selby, Rapid Commun. Mass Spectrom. 11 (1997) 951.
[4] D.S. Selby, V. Mlynski, M. Guilhaus, Rapid Commun. Mass Spectrom. 14 (2000) 616.
[5] R.P. Schmid, C. Weickhardt, Int. J. Mass Spectrom. 206 (2001) 181.
[6] M. Lewin, M. Guilhaus, J. Wildgoose, J. Hoyes, B. Bateman, Rapid Commun. Mass Spectrom. 16 (2002) 609.
[7] S.M. Colby, C.W. Baker, J.J. Manura, Proceedings of the 41st ASMS Conference on Mass Spectrometry and Allied Topics, San Francisco, CA, 1996.
[8] D.A. Dahl, SIMION 3D 7.0, Scientific Instrument Services Inc., Boise Idaho, 2000.
[9] M. Abd El Rahim, R. Antoine, L. Arnaud, M. Barbaire, M. Broyer, C. Clavier, I. Compagnon, P. Dugourd, J. Maurelli, D. Rayane, Rev. Sci. Instrum. 75 (2004) in press.
[10] P. Dugourd, I. Compagnon, F. Lepine, R. Antoine, D. Rayane, M. Broyer, Chem. Phys. Lett. 336 (2001) 511.
[11] W.C. Wiley, I.H. McLaren, Rev. Sci. Instrum. 26 (1955) 1150.